Synthesis of patterned PVDF ultrafiltration membranes: spray-modified non-solvent induced phase separation

Ayesha Ilyas[a], Matthias Mertens[a], Stijn Oyaert[a] and Ivo F.J. Vankelecom[a]*

[a]*Membrane Technology Group (MTG), Division cMACS, Faculty of Bioscience Engineering, KU Leuven, Celestijnenlaan 200F, Box 2454, 3001 Leuven, Belgium*

**Corresponding author: e-mail: ivo.vankelecom@kuleuven.be*

Abstract

Patterned membranes have been attractive for the mitigation of fouling in membrane processes, but existing patterning methods are rather in-effective in terms of scalability and performance due to pore-size reduction and patterning at the non-selective membrane side. Polyvinylidene fluoride (PVDF) was used now to synthesize patterned membranes via the spray-modified non-solvent induced phase separation (s-NIPS), a recently developed technique that avoids the current drawbacks of patterned membranes. However, PVDF intrinsically suffers from a slow phase separation, while very fast fixation of the patterns is crucial with this synthesis method. Therefore, the casting solution was optimized towards an accelerated process of phase inversion by systematically studying the effect of polymer concentration, addition of poly(vinylpyrrolidone) (PVP), addition of non-solvent (H_2O) and use of different casting solvents for adequate patterning of the membranes. SEM analysis and pure water permeance of the synthesized membranes assessed the homogeneity and pattern formation for each membrane. The most optimal casting solution composition comprised of 20 wt% PVDF, 6.7 wt% PVP and 1 wt% H_2O which resulted in homogenously patterned PVDF membranes. The optimized patterned membrane showed a 9 fold increase in PWP as compared to the reference flat membrane thanks to the addition of PVP and H_2O as well as the additional surface area. In the filtration of proteins, the water permeance of the membranes improved drastically (+140%) upon patterning with only a moderate loss of BSA rejection (from 90% to 71%) as compared to the corresponding flat membrane. Realisation of patterning via the s-NIPS method resulted in a higher effective membrane surface area combined with an increased membrane porosity. Reduced flux decline of the patterned membrane (52%) as compared to the flat membrane (62%) during continuous BSA filtration also proved the anti-fouling potential of the created patterns.

Keywords: patterned membranes, polyvinylidene fluoride, non-solvent induced phase separation, casting solution optimization, fouling, phase inversion

1. Introduction

Despite the wide-spread applications of ultrafiltration (UF) in many separation processes [1-5], long-term operations are often still hampered by low fouling resistance and low permeance [6, 7]. A good porous membrane for such processes preferentially has a high permeance, good anti-fouling behavior and excellent chemical resistance to the feed streams and the cleaning agents.

Polyvinylidene fluoride (PVDF) is a common membrane material with applications ranging from microfiltration (MF) to nanofiltration (NF) because of its excellent chemical resistance and thermal stability [8-11]. Surface modification of PVDF membranes has been comprehensively investigated to improve the membrane fouling resistance and permeation by chemical modification method or addition of inorganic particles [10, 12].

Recently, patterned membranes have shed new light on the control of membrane fouling. An extensive amount of studies on surface patterning highlights the anti-fouling potential of such membranes, mostly prepared via phase separation micro-molding (PSμM) or imprinting lithography (IL) [7, 13-21]. In PSμM, a polymer solution is cast on a patterned mold which is then immersed in a non-solvent bath for phase inversion and hence the resulting membrane is released from the mold due to polymer shrinkage. However, this results in patterning of the non-active membrane side [22]. On the other hand, IL uses patterned imprinting molds to transfer patterns above a membrane by varying the applied pressure and temperature for a certain time which reduces the pore size and porosity of the selective layer of the membranes [14]. PES nano-patterned membranes prepared via IL reached a 19-45% higher critical flux but the clean water flux was significantly reduced [19].

Patterned PVDF membranes, prepared via PSμM, showed a 20% increase in water flux and 50% reduced particle deposition on the patterned membranes during waste water treatment, due to the vortex formation in the valley regions, as supported by computational fluid dynamics (CFD) [23-25]. Patterned PVDF flat sheet and hollow fiber membranes showed higher water fluxes and reduced fouling in membrane bioreactor applications [26][27].

In a recent study by our group, patterned flat-sheet membranes were synthesized via sprayed non-solvent induced phase separation (s-NIPS) [28]. This one-step method combines the use of 3D printed casting knives and non-solvent spraying with the conventional NIPS method [22, 29]. In NIPS, addition of non-solvent induces demixing of the cast polymer solution which solidifies subsequently [29]. In s-NIPS, non-solvent is sprayed immediately after the passage of the patterned casting knife to rapidly solidify the introduced structures on the polymer film. Unlike PSµM and IL, membranes prepared via s-NIPS have a patterned selective layer with no reduction in pore-size and porosity [28]. The previous study screened the s-NIPS method to prepare polyacrylonitrile (PAN) and cellulose acetate (CA) membranes, which showed 3× and 50× higher permeances than the respective corresponding non-patterned membranes [28].

In this work, the s-NIPS technique was further developed to allow use of PVDF, a very popular polymer for membrane preparations, but known to undergo a much slower phase-inversion process [12, 27]. Patterning such polymer systems with slow phase inversion is challenging with the s-NIPS preparation method due to re-flow of pattern features on the polymer film before effective solidification of these shapes [29]. Hence, this study systematically investigates the effect of polymer concentration, different casting solvents, additive and non-solvent in the casting solution to create homogenous surface patterns on the PVDF membranes by accelerating the phase separation and polymer solidification during the phase inversion process. The pattern formation, homogeneity and performance of resulting membranes were characterized via SEM and pure water permeances (PWP). Furthermore, the characteristics of the optimized corrugated PVDF membranes were compared to their counterpart non-patterned membranes.

2. Materials and methods

2.1. Construction and characterization of patterned casting knife

CAD designs for the corrugated casting knife was created using AutoCAD 2018 (Autodesk Inc, San Rafael, USA) (*Table 1*). Afterwards, the patterned casting knife was 3D printed by means of a photo polymerization based printer (Objet30 Prime, Stratasys Ltd, Eden Prairie, USA) using a resin material (VeroWhitePlusTM RGD835, Stratasys Ltd, Eden Prairie, USA) and was further characterized via light microscopy (LM, BX51, Olympus).

Table 1. Designed geometry and dimensions of 3D printed patterned casting knife

* a = pattern height, b = pattern width, c = pattern distance.

Pattern shape	Designed pattern height = a (µm)	Designed pattern geometry
Rectangular	1500	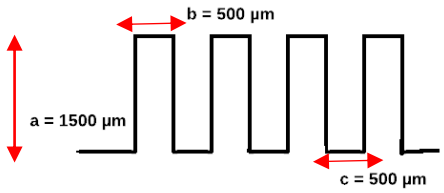

Fig. 1 shows the LM image of the 3D-printed patterned casting knife. The casting knife was produced with an accuracy of ± 195 µm.

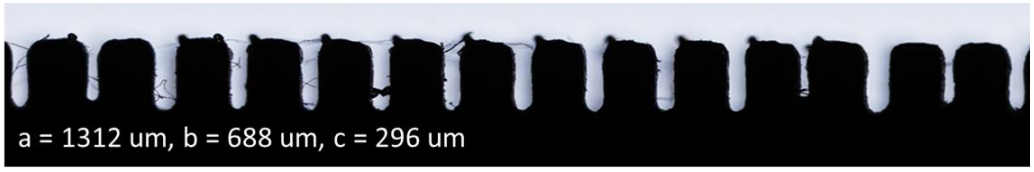

Fig. 1. Light microscopic image of the 3D printed, patterned casting knife *a = pattern height, b = pattern width, c = pattern distance.

2.2. Casting solution preparation and characterization

In order to prepare PVDF-based casting solutions, polymer powder (MW: 543 kDa, Sigma Aldrich, Belgium) was dried overnight at 100 °C to remove any moisture before solution preparation. Polymer solutions were prepared by dissolving five different weight percentages of PVDF in dimethyl formamide (DMF, > 99.9% pure, Acros Organics, Belgium). Afterwards, de-ionized (DI) water was used as non-solvent and poly(vinylpyrrolidone) (PVP, MW: 10 kDa, Sigma Aldrich, Belgium) as additive. Different PVDF (14-22 wt%), PVP (0-9 wt%) and H_2O (0-2 wt%) concentrations were used and solvent was added until a casting solution with total mass of 30 g was obtained. The mixture was stirred overnight to ensure the complete polymer dissolution. When dissolved, the solutions were degassed in a vacuum oven for 10 min after which they were placed in a fume hood for 30 h to be completely degassed. The solvent evaporation during the degassing in the vacuum oven was investigated, and could be neglected. The viscosity of some of the solutions was measured by a stress-controlled rheometer (Anton Paar, Physica MCCR 501) with a cone-plate configuration. A blocker was used to prevent solvent evaporation and the temperature

was set at 20 °C. The viscosity values were taken at a shear rate of 0.1 s^{-1}. *Table 2* shows the composition of all casting solutions prepared during this study.

Table 2. List of different casting solution compositions synthesized during this study.

#	Membrane code	PVDF (wt%)	PVP (wt%)	H_2O (wt%)
1	P14	14	-	0
2	P16	16	-	0
3	P18	18	-	0
4	P20	20	-	0
5	P22	22	-	0
6	$P14^{PVP}$	14	4.7	0
7	$P16^{PVP}$	16	5.4	0
8	$P18^{PVP}$	18	6	0
9	$P20^{PVP}$	20	6.7	0
10	$P22^{PVP}$	22	7.4	0
11	$P14^{PVP\_W}$	14	4.7	1
12	$P16^{PVP\_W}$	16	5.4	1
13	$P18^{PVP\_W}$	18	6	1
14	$P20^{PVP\_W}$	20	6.7	1
15	$P22^{PVP\_W}$	22	7.4	1

2.3. Membrane synthesis and characterization

A flat membrane (code: F_{NS}) was prepared via the conventional NIPS method [22], as a reference membrane. For synthesis of the patterned membranes, each patterned casting knife was attached to the s-NIPS casting setup with the wet-film thickness kept at 200 µm and a casting speed at 1.28 m/min. After the passage of the knife, DI water was sprayed immediately as shown in *Fig. 2*. After casting and spraying, the film was immersed in a DI water coagulation bath for complete phase separation. More details on the setup are reported elsewhere [28]. A flat-sprayed membrane (code: F_S) was also prepared by simultaneous casting and spraying the film without any patterns. Membranes prepared in this study will be referred as their corresponding membrane codes given in Table 2.

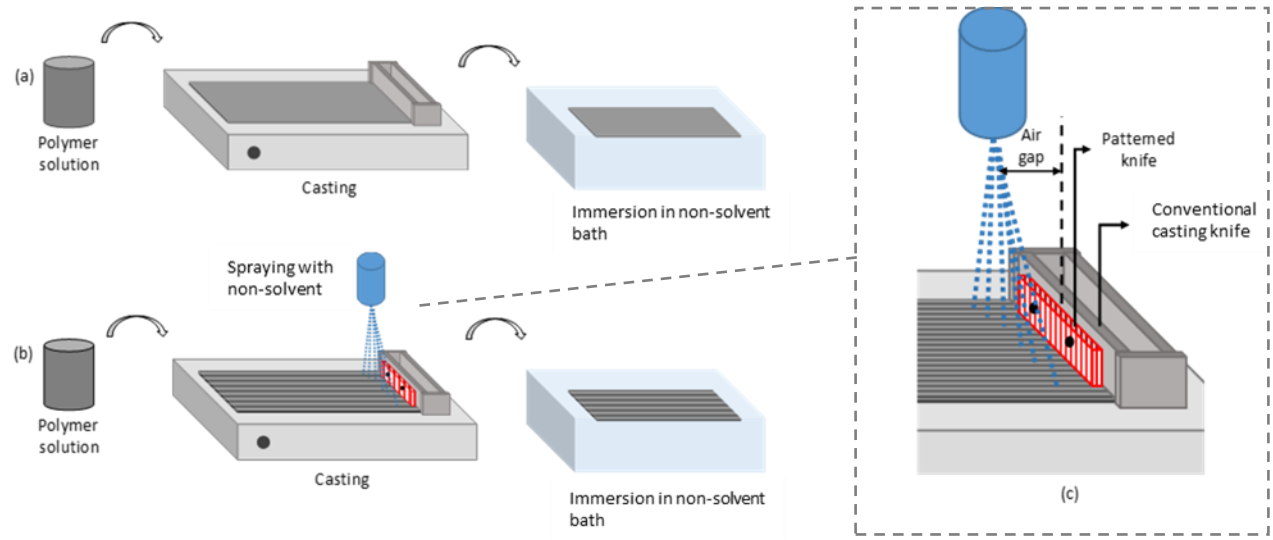

Fig. 2. (a) Conventional NIPS method for synthesis of flat membrane, (b) sprayed NIPS (s-NIPS) and for patterned membrane fabrication, and (c) Detailed scheme of s-NIPS setup [28].

Scanning electron microscopy (SEM, JEOL JSM-6010LV, Tokyo, Japan) and imaging software InTouch (JEOL) was used to assess the patterned membranes' morphologies and dimensions. Air-dried samples were carefully broken after immersion in liquid N_2 and were coated with a gold-palladium layer using a sputtering machine (Auto fine coater, JFC-1300, Tokyo, Japan).

The overall membrane porosity (ε) was measured by the gravimetric method [30], as given by the following equation:

$$\varepsilon\ (\%) = \frac{w_w - w_d}{A \times l \times \rho_w} \times 100 \qquad \text{Eq. (1)}$$

where w_w is the weight of the wet membrane sample weighed after removing the superficial water with filter paper (g), w_d is the weight of membrane sample dried at 60 °C for 24 h in an air-circulating oven (g), A is the effective membrane surface area (cm^2), l is the thickness of membrane sample (cm) and ρ_w is the density of pure water (0.998 g/cm^3).

A high throughput dead-end filtration setup was used to quantify the pure water permeances (PWP) of the membranes [31]. DI water filtrations were carried out at 2 bar with three coupons for each membrane having an active filtration area of 2 cm^2. Prior to filtration, membranes were first

compacted until the flux from the three succesive measurements varied less than 2%. The PWP values were calculated as follows:

$$PWP = \frac{J}{TMP} \; ; \; J = \frac{V}{A\,t} \qquad \text{Eq. (2)}$$

where, J is the flux (L m^{-2} h^{-1}), TMP the trans-membrane pressure (bar), V the permeate volume collected (L), t the filtration time (h), and A the membrane area (m^2).

Rejection (R) studies were conducted using 1 g/L aqueous BSA stirred continously for 3 h prior to each filtration. DI water feed was replaced with BSA solution after 2 h of compaction. BSA concentrations in feed (C_f) and permeate (C_p) were then analyzed using a UV-VIS spectrophotometer (Shimadzu UV-1800) at 287 nm. The rejections were calculated as given in Eq. 3:

$$R\ (\%) = \left(1 - \frac{C_p}{C_f}\right) \times 100 \qquad \text{Eq. (3)}$$

The effect of patterned surface on membrane fouling was studied via stirred dead-end filtration of 1g/L BSA. Three coupons for each membrane sample with 2 cm^2 of active area were tested in the filtration setup (78 cm^2 total area and 15 cm of liquid height at the start of the filtration). The stirring rate in the filtration cell was kept constant at 300 rpm using a 8 cm long magnetic stirrer, to ensure enough mixing above the membrane surface to avoid concentration polarization. The membranes were initially stabilized with DI water at a TMP of 2 bar for 3 h. Compaction was considered stabilized when the differential permeance between three consecutive measurement changed less than 2%. DI water was then replaced by BSA feed solution and the permeance decline with time was recorded till 80 min of filtration for F_{NS}, F_S and patterned membranes.

The mean pore size and pore size distribution of the membranes was determined using a gas-liquid displacement based porosimeter POROLUX™ 1000 (POROMETER, Belgium). Membrane samples (25 mm dia.) were immersed in the wetting liquid (Porefil®, POROMETER, Belgium) (σ = 16 dyn/cm), prior to the testing. The subsequent displacement of the wetting liquid with N_2 takes place with a stepwise pressure scan. The applied pressure and the corresponding gas flow are

measured continuously. The Young-Laplace equation (*Eq. 4*) relates this applied pressure to the corresponding opened pore diameter, as given below

$$P = \frac{4\gamma \cos\theta}{D} \qquad \text{Eq. (4)}$$

where P is the applied pressure, γ the interfacial tension (dyn/cm), θ the contact angle between membrane and wetting liquid (taken as 0°) and D the equivalent pore diameter.

3. Results and discussion

3.1. Effect of polymer concentration

Fig. 3 shows the cross-sectional SEM images of the patterned membranes prepared using different PVDF concentrations. At higher polymer concentrations (i.e. 18-22 wt%), patterns should have been retained better due to the high viscosity and reduced surface tension of the polymer film [28]. However, a clear lack of well-pronounced surface patterns was observed even for the highest polymer concentration (i.e. 22 wt%). The applied patterns on the cast films almost completely disappeared before polymer solidification due to the extremely delayed demixing and/or slow solidification of the PVDF. Cast PVDF films showed 60 min of phase inversion time for complete solidification which led to re-flow of the patterns and only some irregular lines were created.

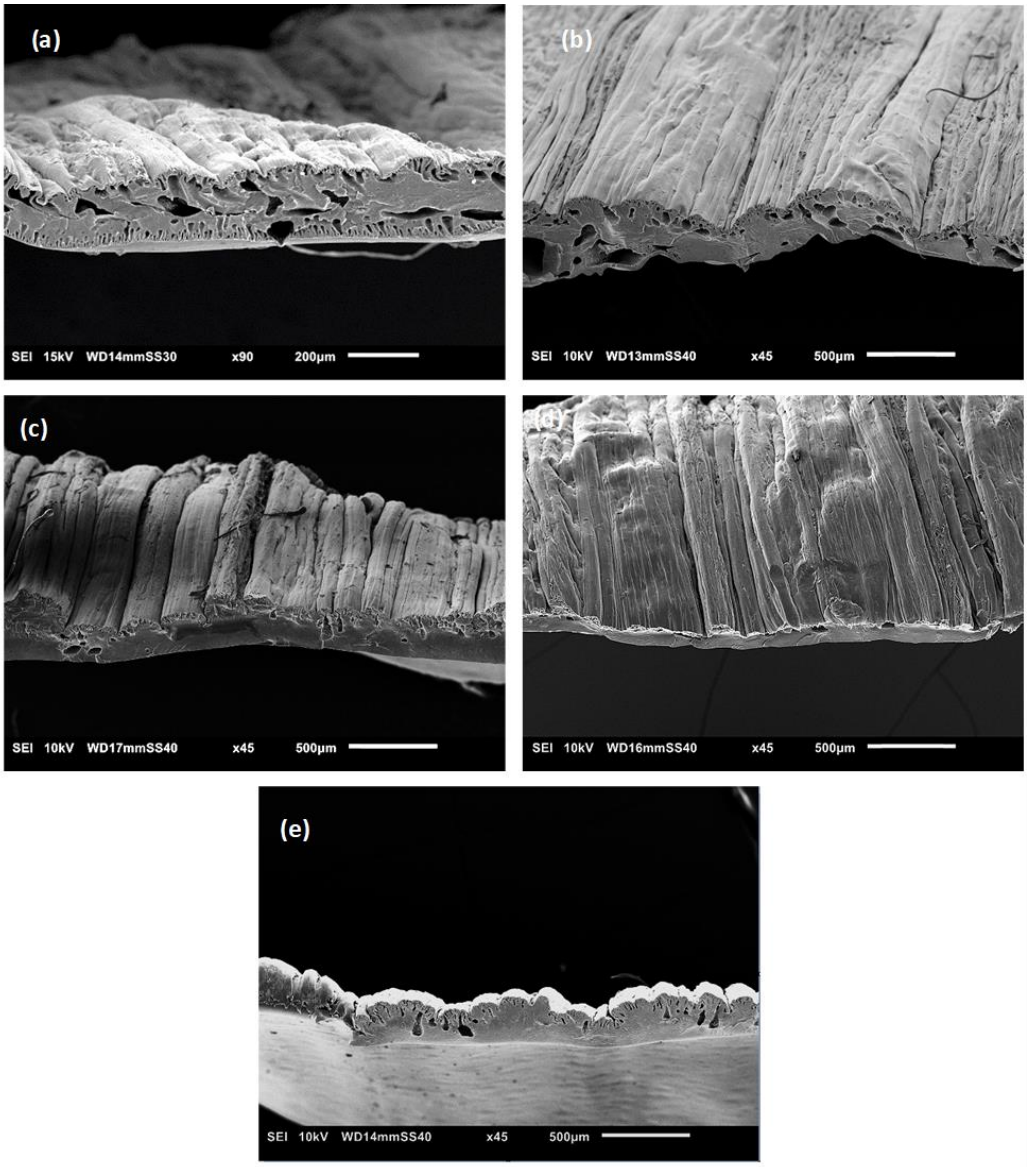

Fig. 3. Cross-sectional SEM images of synthesized PVDF patterned membranes: (a) P14, (b) P16, (c) P18, (d) P20, and (e) P22.

The PWP for these membranes (*Fig. 4*) clearly decreases with increase in PVDF concentration. This confirms the absence of pattern formation as the corresponding non-patterned membranes would exhibit a similar decrease in permeance [10]. *Fig. 4 (b)* shows the decrease in membrane bulk porosity with increase in PVDF concentration, which further explains reduced PWP and confirms no-pattern formation.

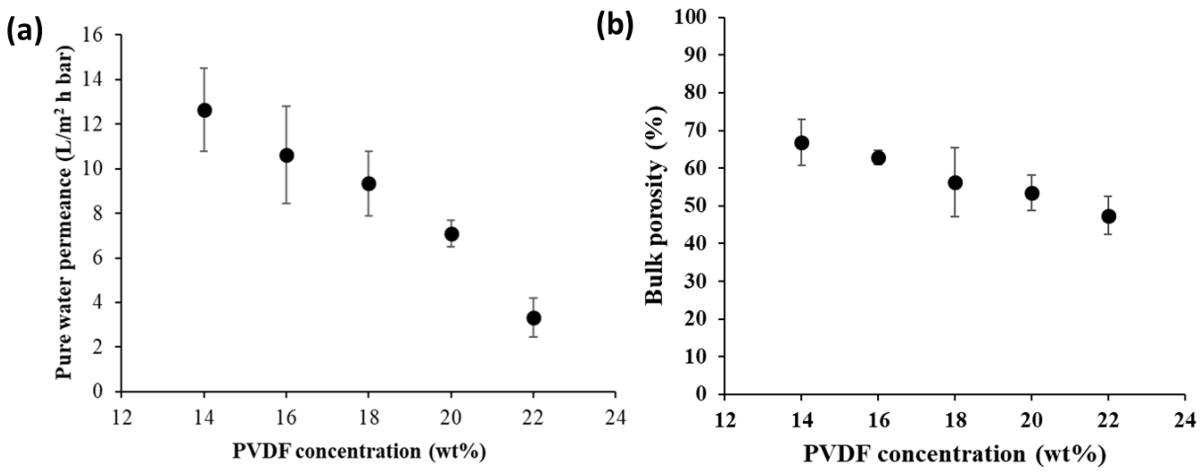

Fig. 4. (a) Pure water permeance and (b) porosity of patterned membranes with PVDF concentration in the casting solution ranging from 14 wt% to 22 wt% in DMF.

3.2. Effect of PVP addition

The results from *Figs. 3 and 4* emphasize the inability to form patterns on a PVDF-based membrane using only higher PVDF concentrations. In order to further increase the viscosity of the polymer casting solution and to accelerate the phase separation, PVP was used as an additive [32], added as 1/3rd of the PVDF concentration in each casting solution [33, 34]. The addition of PVP resulted in a clear increase in solution viscosity from 13.7 ± 0.5 Pa.s to 31.4 ±1.5 Pa.s for a 20 wt% PVDF casting solution. SEM images (*Fig. 5)* also showed a clear increase in membrane porosity since the PVP acts as a pore-former [32]. For lower PVDF concentrations, the addition of PVP did not result in a significant effect on pattern formation, while, on the other hand, patterns appeared on membranes cast from higher PVDF concentrations. As PVP has a non-solvent character, the accelerated liquid-liquid demixing due to reduced thermodynamic stability of the casting solution also have contributed to the improved pattern formation in addition to the increased viscosity [35]. The P22^{PVP} patterned membrane preserved the applied corrugations well with a mean corrugation height of 270 ± 15 μm. The P20^{PVP} membrane also showed some patterns but less pronounced than for P22^{PVP}. Hence, the casting solution with higher PVDF and PVP concentrations (20 wt% - 22 wt%) seem to have the optimal concentration to achieve decent surface patterns.

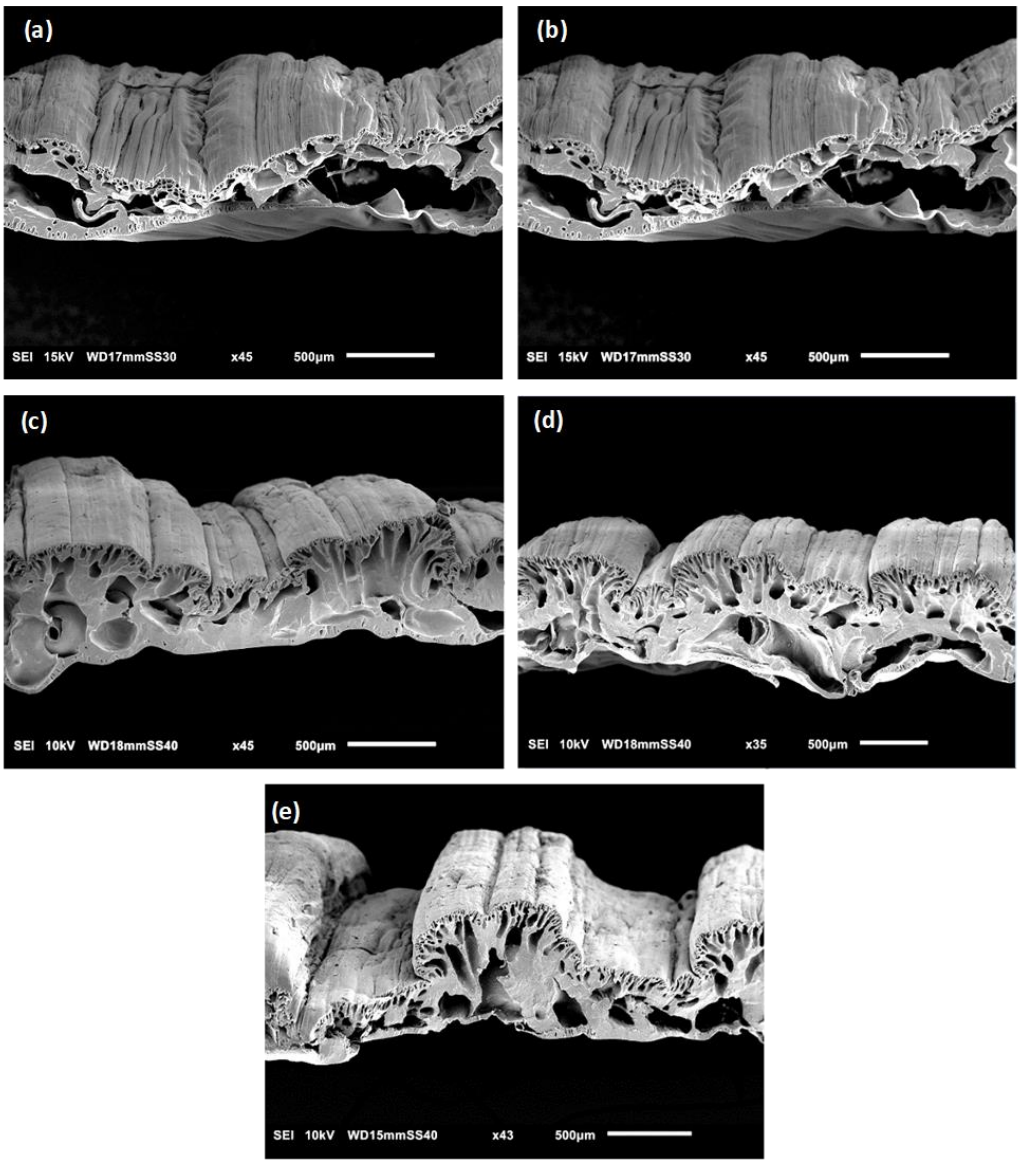

Fig. 5. SEM cross-sectional images of (a) $P14^{PVP}$, (b) $P16^{PVP}$, (c) $P18^{PVP}$, (d) $P20^{PVP}$, and (e) $P22^{PVP}$ patterned membranes.

Fig. 6 shows the opposite trend as in *Fig. 4*: a positive relation was now found between the PWP and the polymer-additive concentration. This observation is in line with literature stating that PVP addition results in an increased membrane porosity [33]. However, it must be noted that the increase in PWP by adding PVP was significantly more pronounced for the higher PVDF concentrations as compared to the lower concentrations. Evaluating the membrane morphology (*Fig. 5*), additional evidence for the cause of this augmented PWP was found. Significantly better pronounced corrugated structures were observed as the PVDF-PVP concentration was increased in the casting solution, thus increasing the effective active surface area of the membrane.

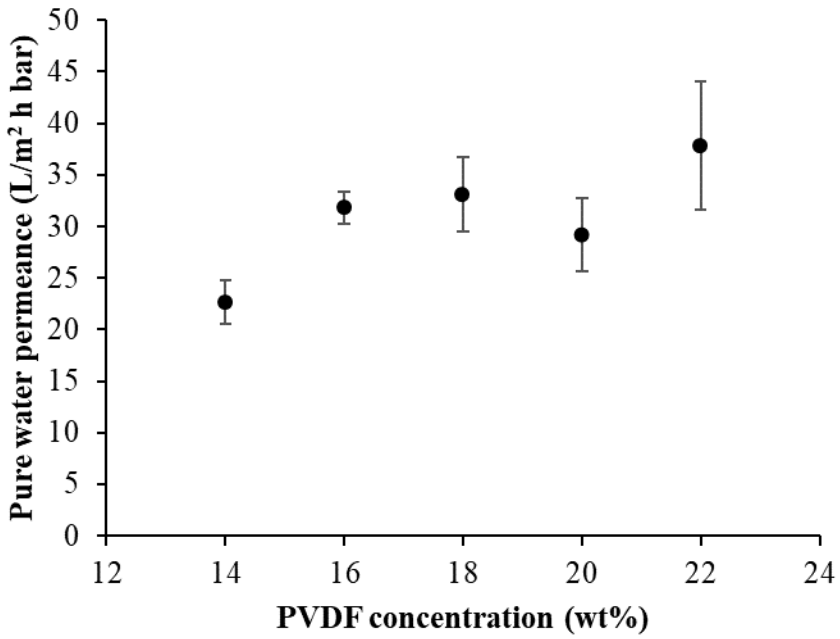

Fig. 6. PWP of patterned membranes with PVDF concentrations ranging from 14 wt% to 22 wt% and a PVP/PVDF ratio of 1/3 in DMF.

3.3. Effect of adding non-solvent

To further tune the polymer-additive system towards faster phase separation to achieve even better and well-reproducible surface patterning, the addition of H_2O as non-solvent was assessed [36]. Presence of non-solvent will result in faster fixation of the applied patterns, resulting in membranes with a more porous top-layer and a macrovoid sub-layer. To achieve this, 1 wt% and 2wt% DI water was added in the casting solutions. For 2 wt% of H_2O, the casting solutions with higher PVDF concentrations became too viscous already to be cast. As a result, 1 wt% H_2O was added to each casting solution with different PVDF-PVP concentrations.

As evident from the SEM images in *Fig. 7*, more homogenous and very pronounced patterns for higher PVDF-PVP concentrations were observed by adding this 1 wt% H_2O to the previous casting solutions. The addition of non-solvent led to a drastic increase in solution viscosity from 31.4 ± 1.5 Pa.s for $P20^{PVP}$ to 2660 ± 0.1 Pa.s for $P20^{PVP\_W}$, respectively. The time required for the transparency of the cast film to fully disappear, was significantly reduced to 20 min with the addition of PVP and H_2O. Although better patterning was achieved for membranes with the highest PVDF-PVP concentration ($P22^{PVP\_W}$), these patterns were difficult to reproduce without any defects due to highly viscous casting solution. Hence, the casting solution with 20 wt% PVDF, 6.7

wt% PVP, 1 wt% H_2O and remaining DMF was considered as the optimal casting solution which resulted in the pattern height of 320 ± 15 µm.

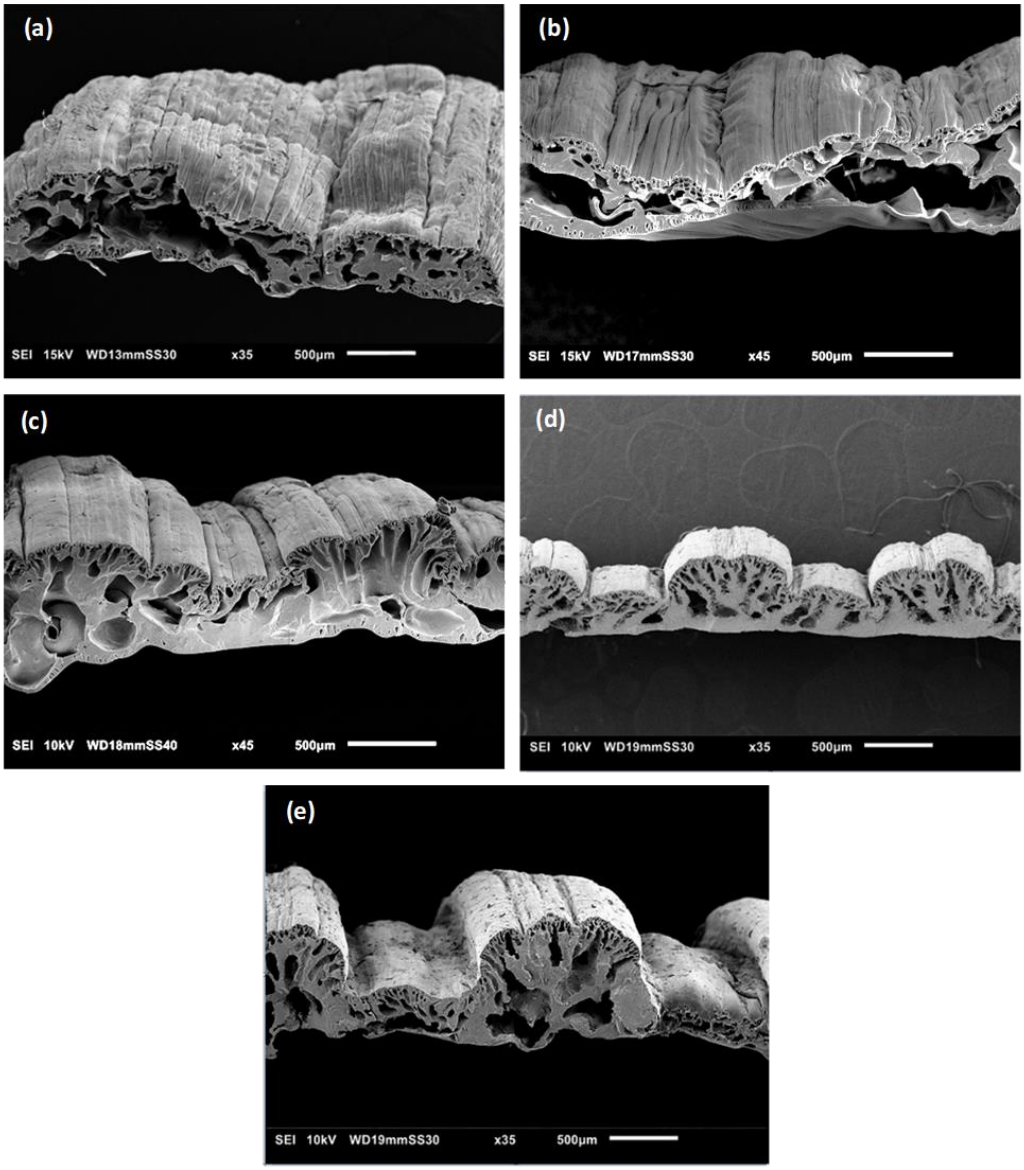

Fig. 7. SEM cross-sectional images of (a) $P14^{PVP\_W}$, (b) $P16^{PVP\_W}$, (c) $P18^{PVP\_W}$, (d)$P20^{PVP\_W}$, and (e) $P22^{PVP\_W}$ patterned membranes.

As hypothesized earlier, a further increase in PWP was observed due to the addition of non-solvent to the polymer casting solution (*Fig. 8)*. However, the membranes with low PVDF concentrations (14 wt% - 18 wt%) showed nearly similar permeances, mainly due to the complete absence of patterns. Addition of PVP and H_2O leads to more instantaneous demixing due to the reduced thermodynamic stability of dope solution, thus increasing porosity. Therefore, the membranes with

well pronounced corrugations (i.e, 20 wt% and 22 wt% PVDF), showed a considerably higher PWP compared to the corresponding membranes without any additives (i.e. H_2O and PVP). This higher PWP can be correlated to the increased membrane surface area from these well pronounced patterns as well as the increased porosity due to the pore former and faster phase separation *(Figs. 4 (b) and 8 (b))*. For example, the well-patterned $P20^{PVP\_W}$ membrane showed a 9-fold increase in PWP as compared to the P20 membrane. Hence, the optimum casting solution composition of 20 wt% PVDF, 6.7 wt% PVP and 1 wt% H_2O was further used in this study to synthesize the corrugated PVDF membranes.

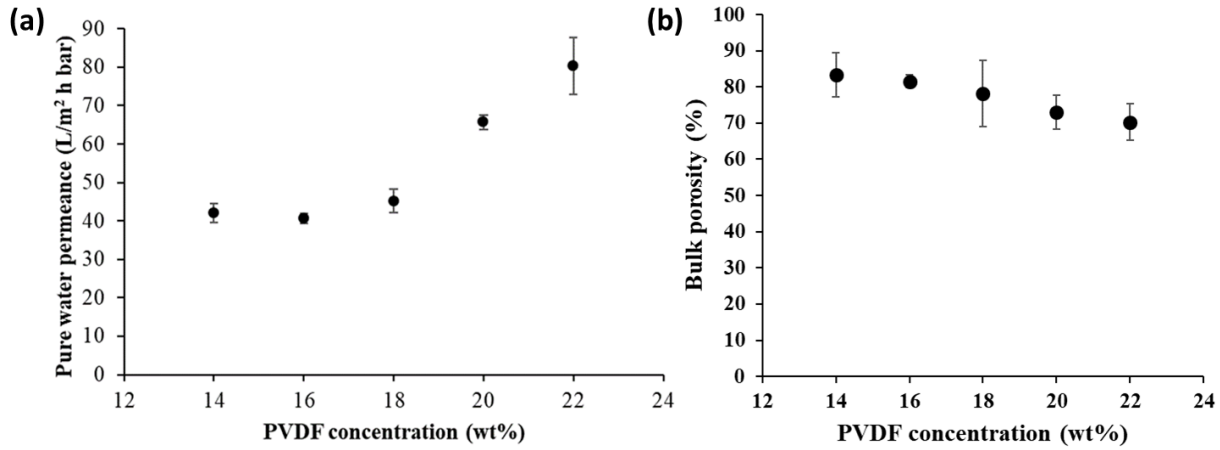

Fig. 8. (a) PWP and (b) porosity of membranes cast from solutions with PVDF concentrations ranging from 14 wt% to 22 wt% with a PVP/PVDF ratio of 1/3 and 1 wt% H_2O in DMF.

3.4. Effect of different PVP concentration

PVP addition is known to significantly influence the morphology and properties of the corrugated PVDF membranes [34]: finger-like pores appear and the PWP increases. To investigate the optimal PVP concentration with respect to corrugation formation and performance of the resulting membranes, a membrane series was synthesized consisting of 20 wt% PVDF casting solutions in DMF with 1 wt% H_2O and a PVP concentration varying from 1 wt% to 9 wt%.

The casting solutions logically became more viscous when a higher additive concentration was used. *Fig. 9* shows the cross-sectional SEM images of these membranes. The support layer contained more finger-like pores and the patterns became more pronounced and upright with increased PVP concentration. For 1 wt% and 3 wt% PVP, the surface patterns largely disappeared before solidification, but well-corrugated membranes were obtained for PVP concentrations of 6

wt% and 9 wt%. Interestingly, a mean pattern height of 315 ± 10 µm was obtained for 6 wt% PVP while the membrane with 9 wt% PVP showed a mean pattern height of 230 ± 9 µm. Thus, despite the increased viscosity for the 9 wt% PVP membrane, the corrugations were less pronounced due to the kinetic hindrance of the viscous casting solution and increased level of polymer chain entanglement which hindered the PVP leaching out and delayed the demixing process.

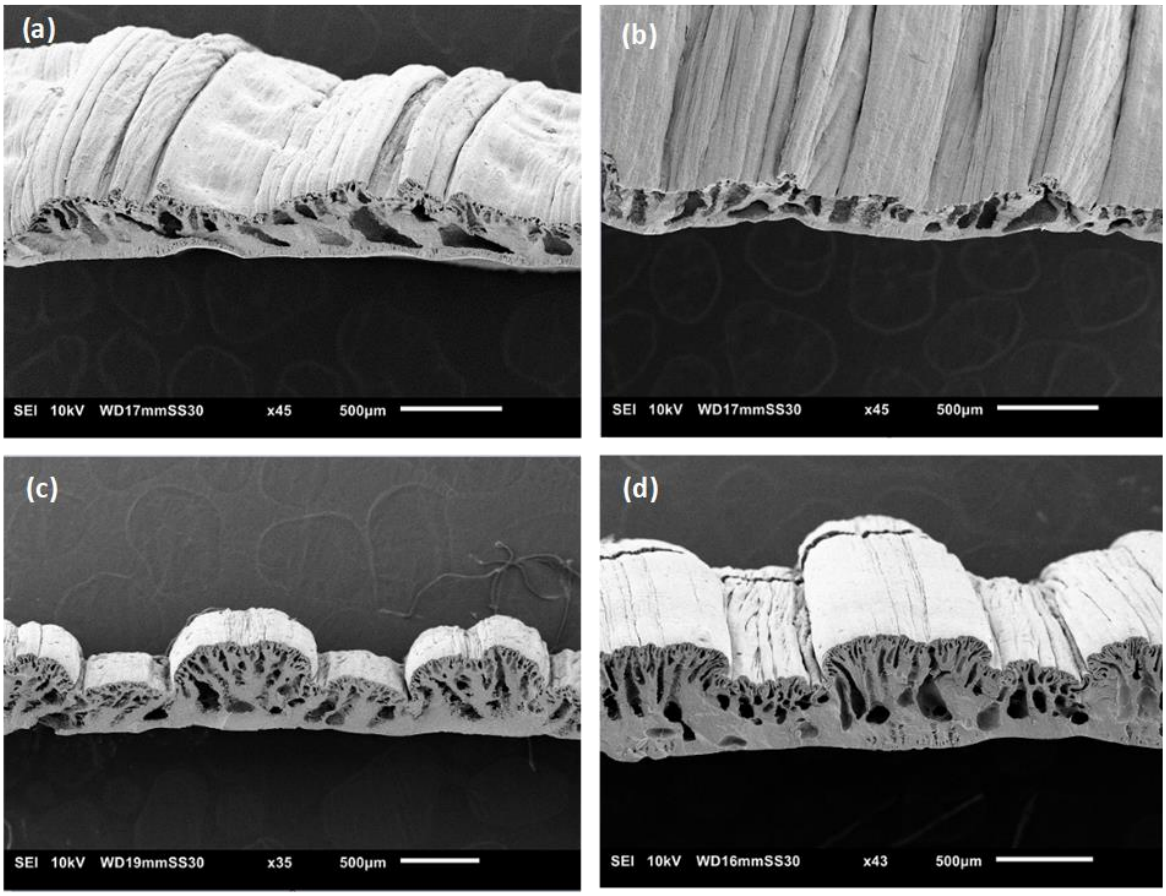

Fig. 9. Cross-sectional SEM images of corrugated PVDF/DMF membranes cast from solutions of 20 wt% PVDF, 1 wt% H_2O in DMF with different PVP concentrations of (a) 1 wt%, (b) 3 wt%, (c) 6 wt%, and (d) 9 wt%.

The large impact of PVP on pore morphology and corrugations can also be observed in the PWP (*Fig. 10 (a)*). The PWP reaches a maximum for a PVP concentration of 6 wt% for Rec_{1500} membranes. It is clear that there is an optimal concentration for this high MW additive with respect to the PWP and corrugations. The increased permeance from 1 wt% to 6 wt% can be attributed to the increased porosity *(Fig. 10 (b))* as well as to the increased surface area of the more and more distinct corrugations on the membranes (*Fig. 9*). From 6 wt% to 9 wt% PVP, a sharp decline in

the water permeance can be seen, possibly due to increased polymer chain entanglement with the additive, which led to ineffective leaching of PVP during phase inversion [34]. Therefore, in accordance with literature, an optimal polymer-additive ration of 1/3rd was maintained throughout further research.

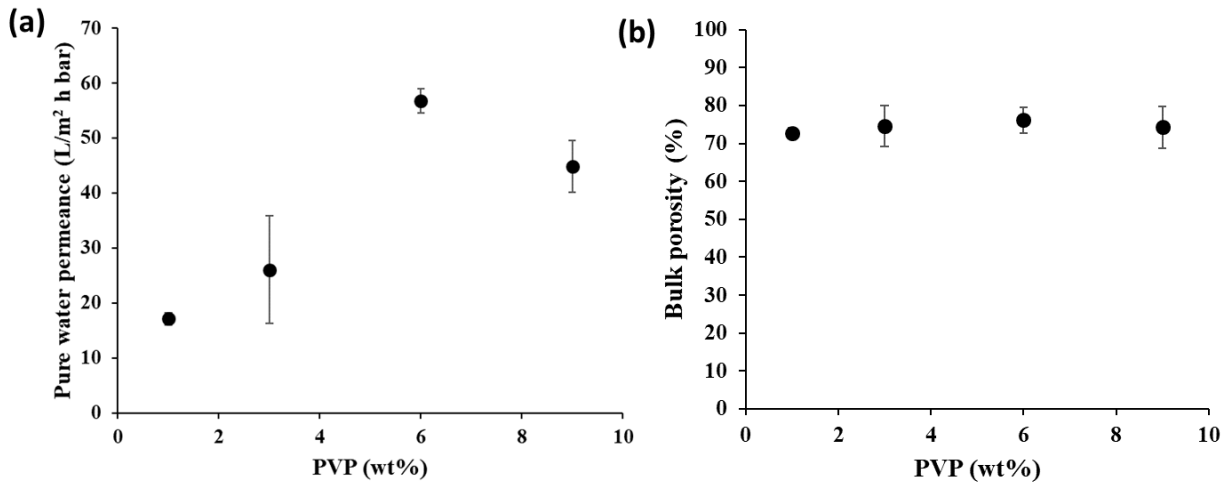

Fig. 10. (a) PWP and (b) porosity of corrugated PVDF/DMF/PVP/H_2O membranes with different PVP concentrations ranging from 1 wt% to 9 wt%.

3.5. Effect of PVDF type

PVDF with higher MW can also affect the pattern formation of the membranes as it can alter the phase inversion kinetics during membrane formation. Hence, Kynar® MG 15A (MW: 1780 kDa), Kynar® 761A (MW: 625 kDa) and Solef® 1015/1001 (MW: 600 kDa) were used for this purpose. For each polymer, the solution composition (PVDF/PVP/H_2O/DMF) was optimized with respect to the patterns on the membranes.

Fig. 11 shows no pattern formation for 15 wt% Kynar® MG15A nor Kynar® 761A PVDF and 1 wt% H_2O composition. The higher MW of these polymers might result in slower phase inversion and hence no patterns could be retained. On the other hand, slightly better patterns with a pattern height of 260 ± 10 µm were obtained for 15 wt% Solef® 1015/1001 with 1 wt% H_2O *(Fig. 11 (c)).* Its further optimization with 5 wt% PVP (*Fig. 11 (d)*) resulted in a further increase in pattern height i.e. 300 ± 15 µm. This can be attributed to the relatively lower MW of Solef 1015/1001, which is comparable to the Sigma Aldrich PVDF, and hence to the relatively low polymer chain entanglement.

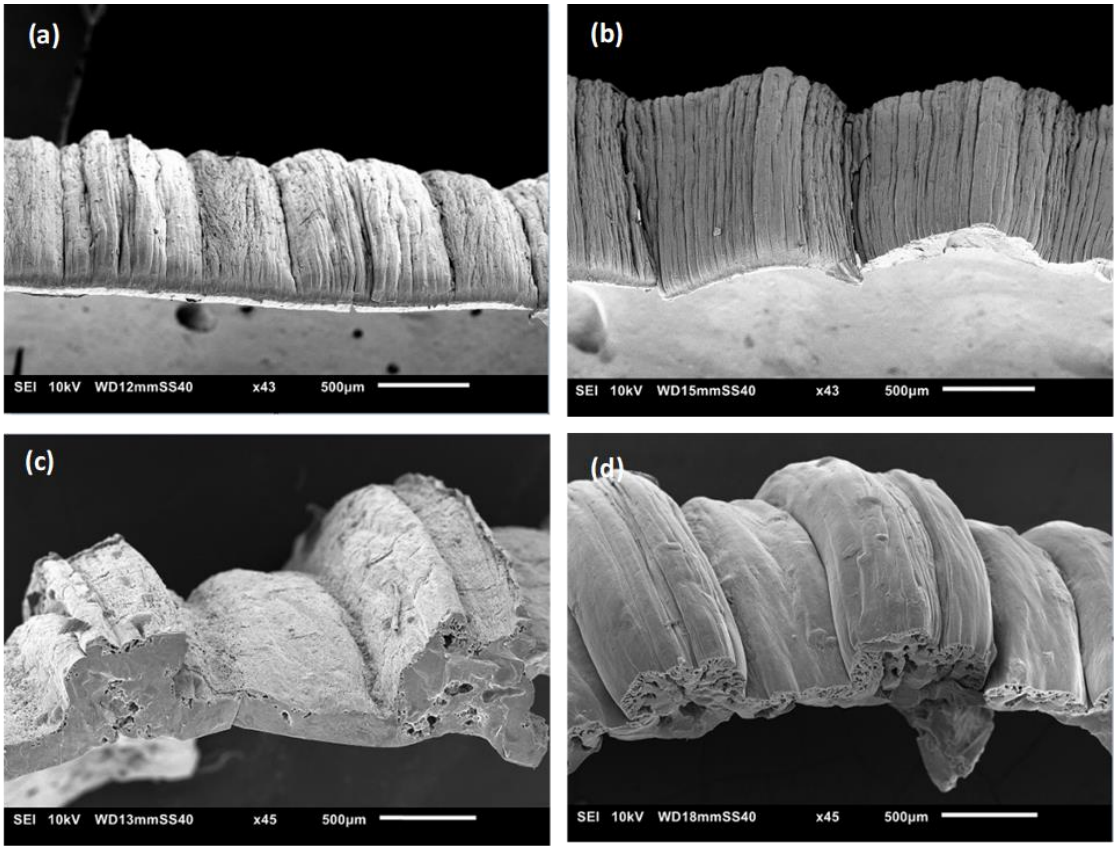

Fig. 11. Cross-sectional SEM images of corrugated PVDF/DMF/H_2O/PVP membranes using different PVDF sources. (a) Kynar MG15A, $P15^{W}$ (b) Kynar 761A, $P15^{W}$ (c) Solef, $P15^{W}$ (d) Solef, $P15^{PVP\_W}$

3.6. Effect of using different casting solvents

In order to move closer to the binodal for quicker phase inversion, the effect of other casting solvents on the pattern formation was investigated. TamiSolve, Triethyl phosphate (TEP), known as green solvents [37], and NMP were selected to replace DMF.

From *Fig. 12*, it can be clearly observed that P15 with TEP and TamiSolve were unable to reduce the phase separation time and could not result in a homogenously patterned membrane. However, for $P15^{PVP\_W}$ with NMP *(Fig. 12 (c))*, patterns started to appear and hence the polymer concentration was further increased to find comparable membrane composition. Hence, $P20^{PVP\_W}$ with NMP (*Fig. 12 (d)*) showed a PWP of 70 ± 5 L/m^2 h bar with a well-pronounced pattern height of 295 ± 15 µm which is fairly comparable to the optimized $P20^{PVP\_W}$ with DMF. A slightly higher PWP can be attributed to the higher miscibility of NMP with the non-solvent, which illustrates that DMF and NMP can be compared fairly well with each other in this context [38].

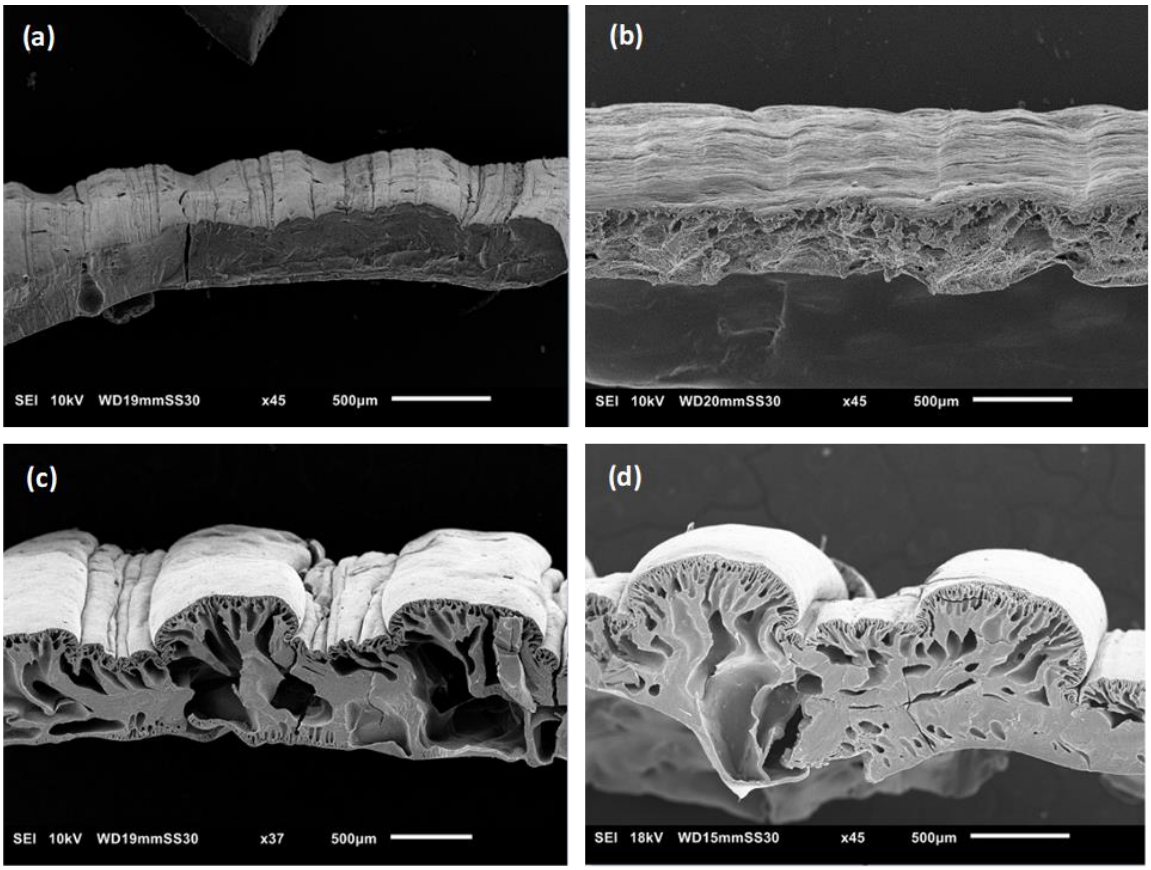

Fig. 12. Cross-sectional SEM images of corrugated PVDF membranes using different casting solvents. (a) P15 with TEP (b) P15 with TamiSolve (c) $P15^{PVP\_W}$ with NMP (d) $P20^{PVP\_W}$ with NMP

3.7. Effect of non-solvent spraying

In order to understand the single effect of the spraying action on the s-NIPS process and hence on the membrane morphology and performance, non-sprayed (i.e., F_{NS}) and sprayed (i.e., F_S) non-corrugated membranes were synthesized for morphological comparison using 20 wt% PVDF, 6.7 wt% PVP and 1 wt% H_2O in DMF. Assessing their cross-sections (*Fig. 13 (a)&(b)*), a clear difference in membrane morphology was observed, in line with the earlier observations for PAN- and CA-based membranes [28]. The F_S membrane exhibited a sponge-like structure with only few and rather small macrovoids, while F_{NS} membrane consisted of many, large finger-like macrovoids. Additionally, *Fig. 13 (c)&(d)* shows a significant increase in surface porosity for the F_S membrane.

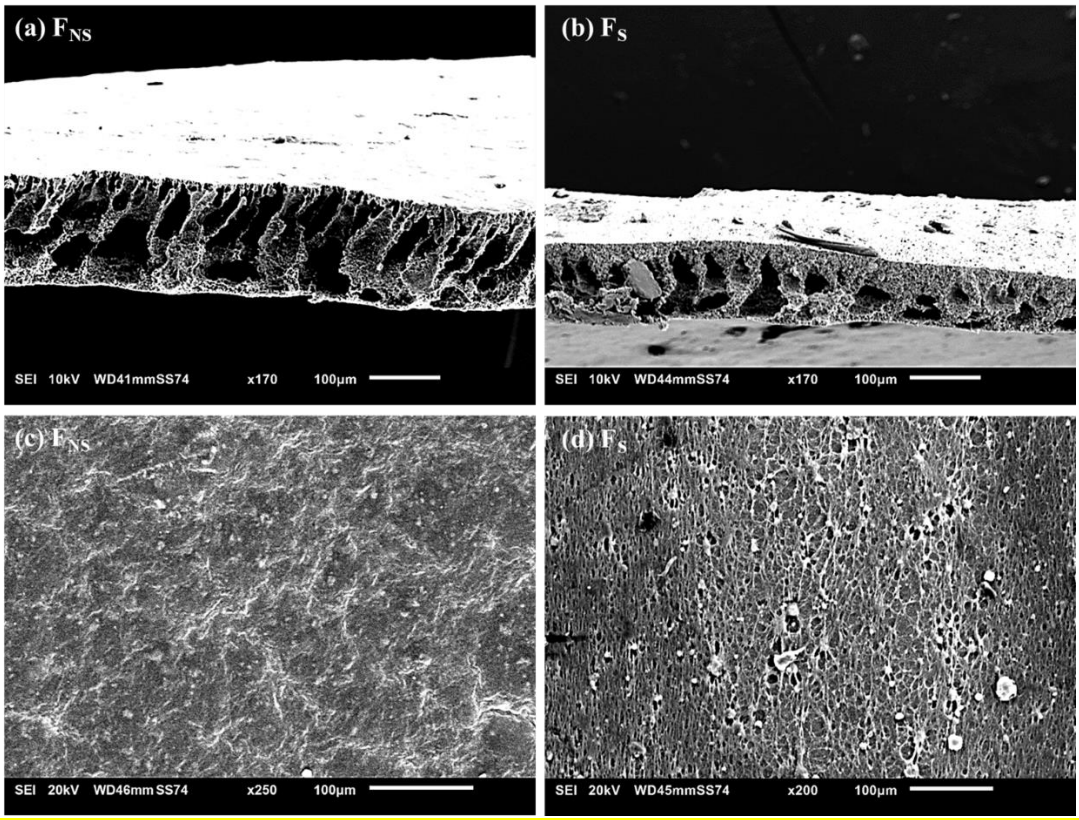

Fig. 13. Cross-sectional SEM images of (a) F_{NS} and (b) F_S membrane; Top surface images of (c) F_{NS} and (d) F_S membrane synthesized using the optimized PVDF casting solution.

Furthermore, the thickness and PWP (*Fig. 14*) for the F_S membranes were also higher than for the corresponding F_{NS} membranes for a set of membranes prepared from casting solutions with different PVDF-concentrations. This also indicates an increase in membrane porosity and pore size due to the non-solvent spraying. A thicker membrane prepared from the same casting solution obviously refers to a more open overall membrane structure *(Fig. 14 (a))*. For the optimized solution of 20 wt% PVDF (F_S), spraying resulted in a 70% increase in membrane thickness and a 40% higher PWP as compared to F_{NS}. The F_S membrane showed a 71 ± 4 % bulk porosity, compared to 59 ± 3 % for F_{NS}. This effect of spraying as such thus also clearly contributes to the overall increase in PWP of the patterned membranes.

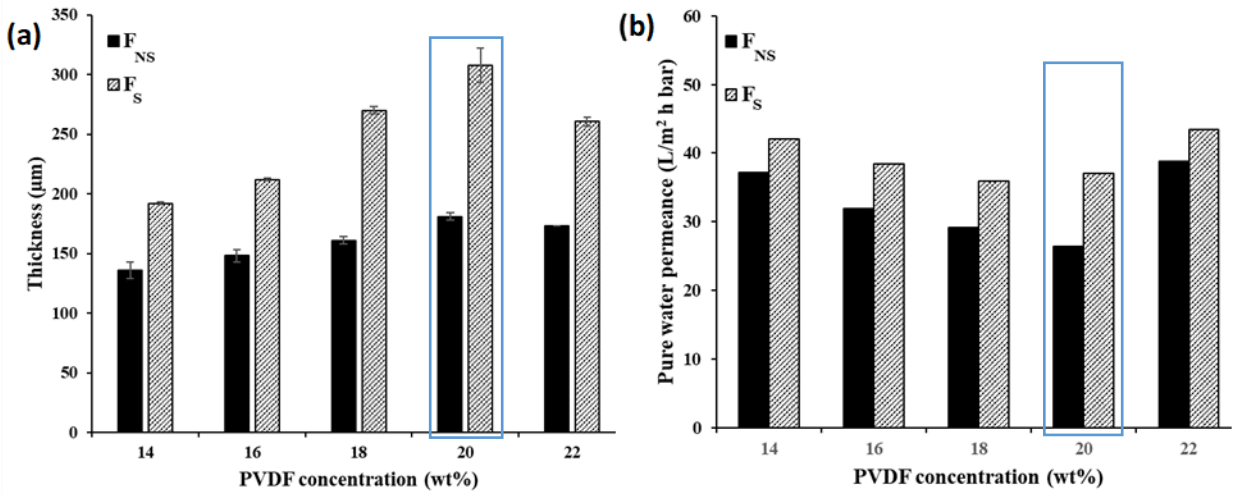

Fig. 14. (a) Membrane thickness and (b) PWP of F_{NS} and F_S membranes cast from different PVDF concentrations.

3.8. Membrane performance

Fig. 15 shows the PWP and BSA rejections for the patterned and flat membranes. The PWP of the patterned membrane correlates well with the additional surface area and shows a 140% higher PWP as compared to the flat membrane. However, simply the spraying of non-solvent also contributes to the overall increase in PWP (+40%) as the experimental PWP for corrugated membranes is higher than the theoretically calculated PWP value, solely based on the added surface area (*Table 3)*. Hence, the combined effect of patterning and spraying during s-NIPS resulted in this improved membrane performance.

This increase in PWP resulted in a lower BSA rejection for corrugated membranes as compared to flat membranes (90%) (*Fig. 15*). As discussed earlier, spraying the non-solvent on a wet polymer film results in a more porous top layer *(Fig. 13 (d))* and therefore a 45% retention. On the other hand, a well-structured corrugated membrane showed 71 ± 4% BSA rejection. Hence, patterned membranes result in substantially higher PWPs with fairly comparable rejections, which confirms the high potential of these membranes in industrial applications.

Table 3. Mathematical and experimental PWP and calculated increase in surface area of PVDF patterned membrane as compared to F_{NS}.

Membrane	Mathematical surface area increase as compared to F_{NS} (%)	Mathematical PWP increase as compared to F_{NS} (%)	Experimental PWP increase as compared to F_{NS} (%)
$P20^{PVP\_W}$	85	125	140

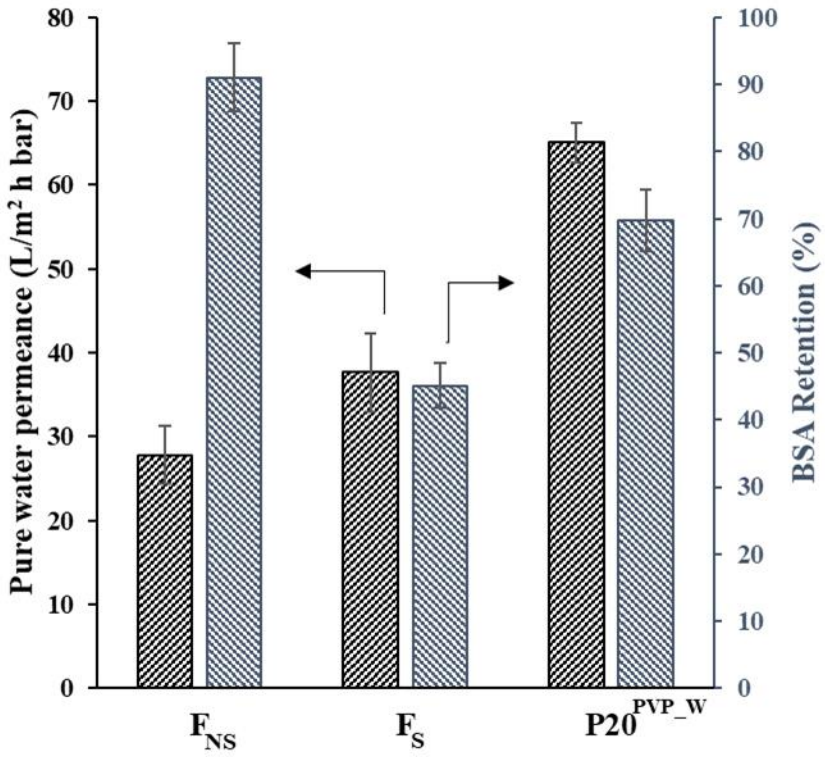

Fig. 15. PWP and BSA rejections for F_{NS}, F_S and patterned membranes.

The influence of spraying and patterning was further investigated by measuring the mean flow pore size and PSD for the patterned and flat membranes, as shown in *Fig.16*. The PSD shifts towards larger pore sizes for the F_S and patterned membranes, which explains their increased permeances and lower rejections as compared to the F_{NS} membrane. The mean pore size for F_{NS} was 283 ± 5 nm, while F_S and $P20^{PVP\_W}$ showed mean pore sizes of 617 ± 157 nm and 735 ± 9 nm, respectively. The broader PSD for the F_S shows a more heterogenous pore size distribution due to the non-solvent spraying. The longer 'tails' of the PSD curves till ~1300 nm and ~2500 nm for patterned and F_S membrane respectively, show the presence of larger pores, which can prevailingly contribute to the increased water fluxes and the reduced rejections. Additionally, the relatively

higher standard deviations, higher surface porosity and broader area under the PSD-curve for the F_S membrane further accounts for the lower BSA rejections as compared to the patterned membrane.

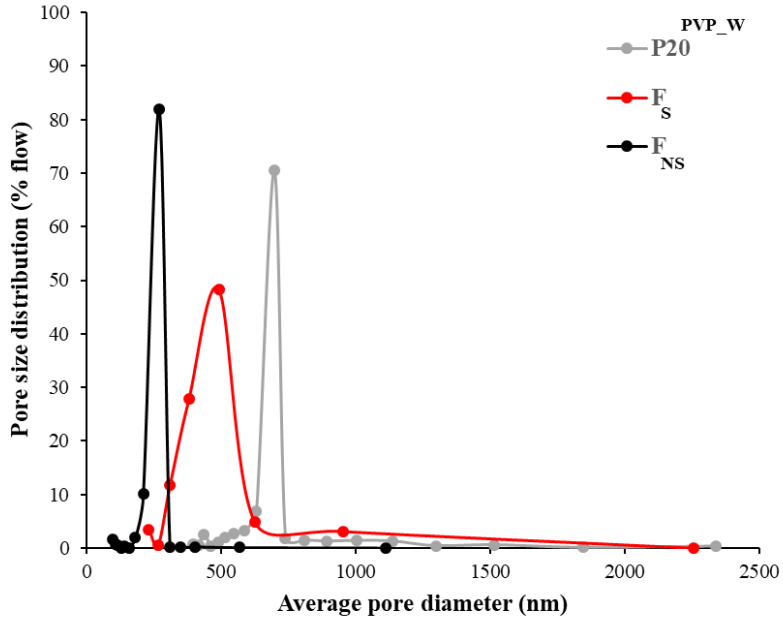

Fig. 16. Pore size flow distribution for F_{NS}, F_S and $P20^{PVP\_W}$ membranes.

Fig. 17 shows the change in permeance with filtration time for flat and patterned membrane using BSA as a model-foulant in the feed in a stirred, dead-end filtration mode. The F_{NS} and F_S membranes showed a loss in permeance i.e., 62% and 72% respectively, whereas the patterned membrane only showed a 52% permeance decrease after 80 min of filtration. For the patterned membranes, the combined effect of a larger effective surface area and presence of surface patterns led to particle deposition in the valley regions, but still leaving the top regions for un-restricted filtration [39]. It should also be noted that the patterned membrane showed a much higher final permeance as compared to flat membranes after 80 min of filtration time: the permeance for the patterned membrane was 12 times higher (22 ± 3 L/m^2 h bar) than for the F_{NS} membrane (1.7 ± 0.2 L/m^2 h bar). The surface patterns can improve the local flow distribution above the membrane during stirring and provide additional effective surface area. However, further investigation is still needed using a cross flow system in order to fully demonstrate the anti-fouling behavior of s-NIPS patterned PVDF membranes.

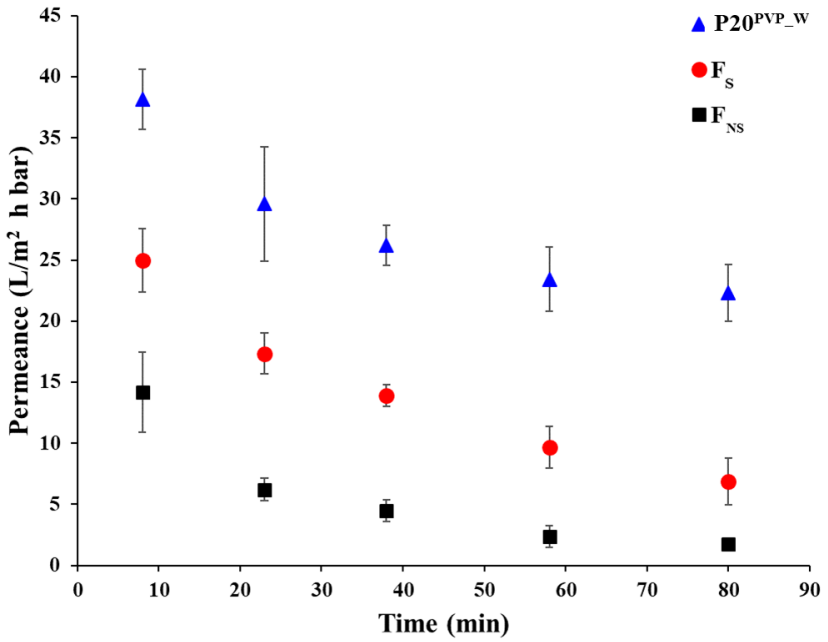

Fig. 17. Permeance decline for F_{NS}, F_S and $P20^{PVP\_W}$ during 80 min filtration using BSA as model foulant.

4. Conclusions

Patterned, flat-sheet PVDF membranes were synthesized via the recently developed s-NIPS method. Because of the intrinsically slow phase inversion process for PVDF, the effects of non-solvent, casting solvent, PVDF type and additives were investigated for different PVDF-concentrations in the membrane casting solutions to realize adequate patterning of the final membranes through accelerated phase inversion. SEM and PWP confirmed the pattern formation and homogeneity of synthesized PVDF membranes. The phase inversion time was significantly reduced from 60 min to 20 min and a 9 fold increase in PWP was observed through a combined effect of addition of PVP, H_2O, patterning, and use of the non-solvent spraying technique. After successful optimization of the casting solution as 20 wt% PVDF, 6.7 wt% PVP and 1 wt% H_2O in DMF, patterned membrane performance was compared to the reference unpatterned membrane. $P20^{PVP\_W}$ showed a 140% higher PWP as compared to the F_{NS} membrane with a 20% decrease in BSA rejection. The increase in PWP for each membrane was only partly due to the added surface of the patterns. An additional increase in PWP was attributed to the change in intrinsic membrane morphology due to non-solvent spraying method, which led as such already to a 40% increased

PWP. Patterned membranes showed less BSA adsorption after 80 min of continuous filtration and a substantially higher final permeance as compared to the flat membrane.

Even for PVDF as a polymer that exhibits an extremely slow phase inversion, the proposed strategy via s-NIPS thus presents new opportunities for designing patterned membranes with significantly higher effective surface areas, higher porosities and induced local turbulences in the feed. They synergistically increase membrane performance and reduce solute adhesion, hence providing a potential platform for producing industrially effective membranes with increased fluxes and longer cleaning-free operations.

5. Acknowledgements

We wish to thank KU Leuven for the financial support in the frame of the projects C1 (C16/17/005), C2 (C24/16/022), and the Belgian Federal Government for an IAP grant. Research Foundation Flanders (FWO) is acknowledged for the research project funding G084818N. We also would like to acknowledge Dr. Anja Vananroye (Soft Matter, Rheology and Technology Section, Dept. of Chemical Engineering, KU Leuven) for the viscosity measurements.

6. References

[1] K. Hendrix, M. Vaneynde, G. Koeckelberghs, I.F. Vankelecom, Synthesis of modified poly (ether ether ketone) polymer for the preparation of ultrafiltration and nanofiltration membranes via phase inversion, Journal of membrane science, 447 (2013) 96-106.

[2] W. Wei, H. Zhang, X. Li, H. Zhang, Y. Li, I. Vankelecom, Hydrophobic asymmetric ultrafiltration PVDF membranes: an alternative separator for VFB with excellent stability, Physical Chemistry Chemical Physics, 15 (2013) 1766-1771.

[3] H.-J. Li, Y.-M. Cao, J.-J. Qin, X.-M. Jie, T.-H. Wang, J.-H. Liu, Q. Yuan, Development and characterization of anti-fouling cellulose hollow fiber UF membranes for oil–water separation, Journal of Membrane science, 279 (2006) 328-335.

[4] Z. Ademovic, D. Klee, P. Kingshott, R. Kaufmann, H. Höcker, Minimization of protein adsorption on poly (vinylidene fluoride), Biomolecular engineering, 19 (2002) 177-182.

[5] J. Mansouri, S. Harrisson, V. Chen, Strategies for controlling biofouling in membrane filtration systems: challenges and opportunities, Journal of Materials Chemistry, 20 (2010) 4567-4586.

[6] A. Nabe, E. Staude, G. Belfort, Surface modification of polysulfone ultrafiltration membranes and fouling by BSA solutions, Journal of membrane science, 133 (1997) 57-72.

[7] S.Y. Jung, K.H. Ahn, Transport and deposition of colloidal particles on a patterned membrane surface: Effect of cross-flow velocity and the size ratio of particle to surface pattern, Journal of membrane science, 572 (2019) 309-319.

[8] F. Liu, N.A. Hashim, Y. Liu, M.M. Abed, K. Li, Progress in the production and modification of PVDF membranes, Journal of membrane science, 375 (2011) 1-27.

[9] M. Tao, F. Liu, L. Xue, Hydrophilic poly (vinylidene fluoride)(PVDF) membrane by in situ polymerisation of 2-hydroxyethyl methacrylate (HEMA) and micro-phase separation, Journal of Materials Chemistry, 22 (2012) 9131-9137.

[10] C. Van Goethem, M. Mertens, I.F. Vankelecom, Crosslinked PVDF membranes for aqueous and extreme pH nanofiltration, Journal of membrane science, 572 (2019) 489-495.

[11] M. Mertens, T. Van Dyck, C. Van Goethem, A. Gebreyohannes, I.F. Vankelecom, Development of a polyvinylidene difluoride membrane for nanofiltration, Journal of Membrane Science, 557 (2018) 24-29.

[12] L. Marbelia, M.R. Bilad, A. Piassecka, P.S. Jishna, P.V. Naik, I.F. Vankelecom, Study of PVDF asymmetric membranes in a high-throughput membrane bioreactor (HT-MBR): Influence of phase inversion parameters and filtration performance, Separation and Purification Technology, 162 (2016) 6-13.

[13] S.T. Weinman, E.M. Fierce, S.M. Husson, Nanopatterning commercial nanofiltration and reverse osmosis membranes, Separation and Purification Technology, 209 (2019) 646-657.

[14] S.H. Maruf, Z. Li, J.A. Yoshimura, J. Xiao, A.R. Greenberg, Y. Ding, Influence of nanoimprint lithography on membrane structure and performance, Polymer, 69 (2015) 129-137.

[15] M. Xie, W. Luo, S.R. Gray, Surface pattern by nanoimprint for membrane fouling mitigation: Design, performance and mechanisms, Water research, 124 (2017) 238-243.

[16] J.H. Jang, J. Lee, S.-Y. Jung, D.-C. Choi, Y.-J. Won, K.H. Ahn, P.-K. Park, C.-H. Lee, Correlation between particle deposition and the size ratio of particles to patterns in nano-and micro-patterned membrane filtration systems, Separation and Purification Technology, 156 (2015) 608-616.

[17] Y.K. Lee, Y.-J. Won, J.H. Yoo, K.H. Ahn, C.-H. Lee, Flow analysis and fouling on the patterned membrane surface, Journal of membrane science, 427 (2013) 320-325.

[18] S.Y. Jung, Y.-J. Won, J.H. Jang, J.H. Yoo, K.H. Ahn, C.-H. Lee, Particle deposition on the patterned membrane surface: Simulation and experiments, Desalination, 370 (2015) 17-24.

[19] S.H. Maruf, A.R. Greenberg, J. Pellegrino, Y. Ding, Critical flux of surface-patterned ultrafiltration membranes during cross-flow filtration of colloidal particles, Journal of membrane science, 471 (2014) 65-71.

[20] S.H. Maruf, L. Wang, A.R. Greenberg, J. Pellegrino, Y. Ding, Use of nanoimprinted surface patterns to mitigate colloidal deposition on ultrafiltration membranes, Journal of membrane science, 428 (2013) 598-607.

[21] O. Heinz, M. Aghajani, A.R. Greenberg, Y. Ding, Surface-patterning of polymeric membranes: fabrication and performance, Current opinion in chemical engineering, 20 (2018) 1-12.

[22] D.-M. Wang, J.-Y. Lai, Recent advances in preparation and morphology control of polymeric membranes formed by nonsolvent induced phase separation, Current Opinion in Chemical Engineering, 2 (2013) 229-237.

[23] Y.-J. Won, J. Lee, D.-C. Choi, H.R. Chae, I. Kim, C.-H. Lee, I.-C. Kim, Preparation and application of patterned membranes for wastewater treatment, Environmental science & technology, 46 (2012) 11021-11027.

[24] Y.-J. Won, D.-C. Choi, J.H. Jang, J.-W. Lee, H.R. Chae, I. Kim, K.H. Ahn, C.-H. Lee, I.-C. Kim, Factors affecting pattern fidelity and performance of a patterned membrane, Journal of membrane science, 462 (2014) 1-8.

[25] Y.-J. Won, S.-Y. Jung, J.-H. Jang, J.-W. Lee, H.-R. Chae, D.-C. Choi, K.H. Ahn, C.-H. Lee, P.-K. Park, Correlation of membrane fouling with topography of patterned membranes for water treatment, Journal of membrane science, 498 (2016) 14-19.

[26] I. Kim, D.-C. Choi, J. Lee, H.-R. Chae, J.H. Jang, C.-H. Lee, P.-K. Park, Y.-J. Won, Preparation and application of patterned hollow-fiber membranes to membrane bioreactor for wastewater treatment, Journal of membrane science, 490 (2015) 190-196.

[27] J.A. Kharraz, M. Bilad, H.A. Arafat, Simple and effective corrugation of PVDF membranes for enhanced MBR performance, Journal of membrane science, 475 (2015) 91-100.

[28] L. Marbelia, A. Ilyas, M. Dierick, J. Qian, C. Achille, R. Ameloot, I.F. Vankelecom, Preparation of patterned flat-sheet membranes using a modified phase inversion process and advanced casting knife construction techniques, Journal of Membrane Science, (2019) 117621.

[29] A.K. Hołda, I.F. Vankelecom, Understanding and guiding the phase inversion process for synthesis of solvent resistant nanofiltration membranes, Journal of Applied Polymer Science, 132 (2015).

[30] J. Mulder, Basic principles of membrane technology, Springer Science & Business Media, 2012.

[31] P. Vandezande, L.E. Gevers, J.S. Paul, I.F. Vankelecom, P.A. Jacobs, High throughput screening for rapid development of membranes and membrane processes, Journal of membrane science, 250 (2005) 305-310.

[32] M.-J. Han, S.-T. Nam, Thermodynamic and rheological variation in polysulfone solution by PVP and its effect in the preparation of phase inversion membrane, Journal of Membrane Science, 202 (2002) 55-61.

[33] M.O. Mavukkandy, M.R. Bilad, A. Giwa, S.W. Hasan, H.A. Arafat, Leaching of PVP from PVDF/PVP blend membranes: impacts on membrane structure and fouling in membrane bioreactors, Journal of Materials Science, 51 (2016) 4328-4341.

[34] L. Marbelia, M.R. Bilad, I.F. Vankelecom, Gradual PVP leaching from PVDF/PVP blend membranes and its effects on membrane fouling in membrane bioreactors, Separation and Purification Technology, 213 (2019) 276-282.

[35] L. Wu, J. Sun, C. He, Effects of solvent sort, PES and PVP concentration on the properties and morphology of PVDF/PES blend hollow fiber membranes, Journal of applied polymer science, 116 (2010) 1566-1573.

[36] A. Mansourizadeh, A. Ismail, Preparation and characterization of porous PVDF hollow fiber membranes for CO2 absorption: Effect of different non-solvent additives in the polymer dope, International Journal of Greenhouse Gas Control, 5 (2011) 640-648.

[37] T. Marino, F. Russo, A. Criscuoli, A. Figoli, TamiSolve® NxG as novel solvent for polymeric membrane preparation, Journal of Membrane Science, 542 (2017) 418-429.

[38] S.S. Madaeni, A.H. Taheri, Effect of casting solution on morphology and performance of PVDF microfiltration membranes, Chemical engineering & technology, 34 (2011) 1328-1334.

[39] W. Choi, E.P. Chan, J.-H. Park, W.-G. Ahn, H.W. Jung, S. Hong, J.S. Lee, J.-Y. Han, S. Park, D.-H. Ko, Nanoscale pillar-enhanced tribological surfaces as antifouling membranes, ACS applied materials & interfaces, 8 (2016) 31433-31441.